*minerals*

MDPI

*Article*

# Isolation and Characterization of A Novel Iron–Sulfur Oxidizing Bacterium *Acidithiobacillus Ferrooxidans* YQ-N3 and its Applicability in Coal Biodesulfurization

**Wenbo Li [1,2], Qiyan Feng [1,2,*] and Ze Li [1,2]**

[1] School of Environment Science and Spatial Informatics, China University of Mining and Technology, Xuzhou 221116, China
[2] Engineering Research Center of Ministry of Education for Mine Ecological Restoration, China University of Mining and Technology, Xuzhou 221116, China
* Correspondence: fqycumt@126.com

**Abstract:** *Acidithiobacillus ferrooxidans* is a chemotrophic, aerobic, acidophilic, and Gram-negative bacterium that plays a key role in iron and sulfur cycling and has a wide range of applications in the industrial field. A novel *A. ferrooxidans* strain, hereinafter referred to as strain "YQ-N3", was isolated from sediments of a river polluted by acid mine drainage (AMD) of an abandoned mine in Shanxi, China. The whole genome sequencing results revealed that *A. ferrooxidans* YQ-N3 has a 3,217,720 bp genome, which is comprised of one circular chromosome and five circular plasmids (Plasmid A, Plasmid B, Plasmid C, Plasmid D, Plasmid E). Plasmid E, a new plasmid, had not been annotated in the reference database. *A. ferrooxidans* YQ-N3 had a close evolutionary relationship with *A. ferrooxidans* ATCC23270 and *A. ferridurans* JCM18981 and exhibited higher similarity in its genomic structure with *A. ferrooxidans* ATCC23270. Multiple genes related to environmental resistance and iron and sulfur metabolism were predicted from its genome. *A. ferrooxidans* YQ-N3 can remarkably increase the oxidation rate of $Fe^{2+}$ and $S^0$ and enhance the hydrophilicity of $S^0$, which was supported by functional gene analysis and laboratory experiments. The biological desulfurization experiment demonstrated that *A. ferrooxidans* YQ-N3 can reduce the sulfur content in coal by removing pyrite sulfur and organic sulfur.

**Keywords:** *Acidithiobacillus ferrooxidans*; complete genome; comparative genomics; iron–sulfur oxidation; biodesulfurization



**Citation:** Li, W.; Feng, Q.; Li, Z. Isolation and Characterization of A Novel Iron–Sulfur Oxidizing Bacterium *Acidithiobacillus Ferrooxidans* YQ-N3 and its Applicability in Coal Biodesulfurization. *Minerals* **2023**, *13*, 95. https://doi.org/10.3390/min13010095

Academic Editor: Edward J. O'Loughlin

Received: 20 November 2022
Revised: 3 January 2023
Accepted: 5 January 2023
Published: 7 January 2023



## 1. Introduction

*Acidithiobacillus ferrooxidans* (*A. ferrooxidans*) is an aerobic, acidophilic, Gram-negative, chemotrophic prokaryote [1]. This bacterium is widely present in acidic mine soils, puddles, and environments containing iron or sulfur deposits. Its major energy sources are iron, sulfur, and sulfide minerals, and its metabolites include sulfate and $Fe^{3+}$ [2]. Therefore, this bacterium plays a key role in the natural biogeochemical cycles of Fe and S. *A. ferrooxidans* participates in the oxidation of metal sulfide minerals in mining areas via the oxidation of $Fe^{2+}$ and reduced sulfur compounds, resulting in acid mine drainage (AMD) in mining areas. Due to its low pH, high sulfate, and heavy metal contents, AMD can severely impact the surrounding soil and groundwater [3]. In fact, the United States Environmental Protection Agency (EPA) has reported that the environmental risks posed by AMD are second only to global warming and ozone depletion [4]. However, despite considerable efforts to identify the generation mechanisms of AMD and potential removal strategies, little progress has been made toward the development of effective AMD mitigation methods.

Due to its capacity to oxidize $Fe^{2+}$ and reduce sulfur compounds on an industrial scale, *A. ferrooxidans* has been widely applied in bioleaching, biological desulfurization, biosynthesis, and biochemical production [5]. For instance, Lorenzo-Tallafigo et al. developed a

new process for the recovery of lead, silver, and gold from polymetallic sulfide ores using *A. ferrooxidans* and demonstrated that the process was cleaner than using traditional hydrometallurgical methods (e.g., hot brine leaching) [6]. The process included a bio-oxidation stage, where sulfides were oxidized in the presence of extremophiles, followed by pickling and citric acid leaching, after which lead was successfully recovered. Nie et al. isolated *A. ferrooxidans* Z1 from printed circuit board waste and confirmed that *A. ferrooxidans* Z1 was able to extract 96% of copper from waste printed circuit boards at an initial $Fe^{2+}$ concentration of 12 g $L^{-1}$ after seven days [7]. *A. ferrooxidans* can also be used to produce a variety of biomaterials, including schwertmannite, jarosite, iron–sulfur clusters (ISC), and magnetosomes [8]. Additionally, the biological desulfurization of coal would greatly contribute to its clean utilization. Rout et al. reported that *A. ferrooxidans* cells catalyzed the removal of sulfur in both organic and inorganic forms in coal samples, and approximately 79% of the total sulfur was removed from coal samples during a microbiological desulfurization process in a 500 mL flask within 14 days [9]. Currently, most studies on *A. ferrooxidans* have focused on model strains (e.g., ATCC23270), whereas newly discovered *A. ferrooxidans* strains have not been studied in depth. Therefore, examining novel *A. ferrooxidans* strains may provide new insights into the involvement of *A. ferrooxidans* in biogeochemical cycles and its applicability in the biological desulfurization of coal.

In this study, a novel *A. ferrooxidans* strain was isolated from sediments of a river polluted by the AMD of an abandoned mine in Shanxi, China. The whole genome of the newly isolated strain was sequenced, the oxidation features of $Fe^{2+}$, $S^0$, and $FeS_2$ were studied, and the performance of coal desulfurization was also tested. Additionally, the genomic characteristics, the capacity to oxidize iron and sulfur, and the environmental adaptability of the newly discovered strain were analyzed from a comparative and functional genomics perspective. Therefore, this study provides a theoretical basis for studying the formation and processing of AMD, as well as for the development and optimization of industrial applications using *A. ferrooxidans* YQ-N3.

## 2. Materials and Methods

### *2.1. Isolation, Purification, and Identification*

Due to the growth characteristics of *A. ferrooxidans*, Leathen or 9K media are often used during the isolation and purification of this bacterium [10]. In this study, 9K medium was selected for the isolation and purification of *A. ferrooxidans*. The 9K liquid medium is composed of solutions A and B. Solution A is composed of 3.00 g/L $(NH_4)_2{\cdot}SO_4$, 0.10 g/L KCl, 0.655 g/L $K_2HPO_4{\cdot}3H_2O$, 0.50 g/L $MgSO_3{\cdot}7H_2O$, and 0.01 g/L $Ca(NO_3)_2{\cdot}4H_2O$. After the preparation of solution A, the pH of the solution was adjusted to 1.8 with 1:1 concentrated sulfuric acid and sterilized in an autoclave at 121 °C for 20 min. Solution B contains $FeSO_4{\cdot}7H_2O$ and was sterilized using a microporous membrane (d = 0.22 μm). After cooling down to room temperature, Solution A was evenly mixed with Solution B before use. Furthermore, the 9K solid medium contained Solution A, Solution B, and Solution C. Solutions A and B were prepared as described above, whereas solution C was a 7.5 g/L agarose solution. After solution C was heated and dissolved, it was sterilized in an autoclave at 121 °C for 20 min. Once solution A was cooled to approximately 60 °C, it was mixed with Solution B. When the pH was adjusted to 2.0, Solution C was quickly added to the mixture to make a solid medium [11].

The strains used in this study were isolated from sediments of a river polluted by AMD from an abandoned mine in Shanxi, China. Following aseptic procedures, the sediment samples were collected and stored at 4 °C and then transported to the laboratory. Next, 10 g of sediment sample was added to 100 mL of sterile water and the mixture was incubated at 30 °C and 180 r/min for three days. The samples were then filtered to obtain a bacterial solution, which was stored at 4 °C. The bacteria-containing solution was inoculated into an Erlenmeyer flask containing 9K liquid medium at a 10% inoculum volume. Next, the flask was covered with a perforated sealing film (polypropylene, Beckman) and transferred to a constant temperature incubator at 30 °C and 180 r/min for continuous enrichment

culture. Once the bacteria had multiplied until the medium turned reddish–brown, the culture was inoculated into a new 9K liquid medium at a 10% inoculum volume rate, and isolation and purification were performed after 5–6 consecutive enrichments. The enrichment experiments were conducted in triplicate. An alternate solid–liquid culture method was used for the isolation and purification of *A. ferrooxidans*. The gradient dilution method was adopted during the isolation. Sterile sulfuric acid solution (pH = 1.8) was used to dilute the enriched bacterial liquid samples, and each sample was sequentially diluted from the initial concentration 10, $10^2$, $10^3$, $10^4$, $10^5$, and $10^6$ times. Next, 0.2 mL of bacterial solutions at different concentrations was inoculated into the solidified 9K solid medium and evenly coated using a sterile coating rod. After coating, the Petri dish was placed upright in a constant temperature incubator at 30 °C for 10 h, after which the Petri dish was incubated upside down to prevent contamination caused by the backflow of water to the 9K solid medium. Isolation and purification were performed when the liquid medium turned reddish–brown. This process was repeated until pure strains were obtained.

A small amount of bacterial solution was taken after isolation and purification, after which a 1–1.5 cm diameter bacterial smear was evenly spread on a glass slide with a sterile inoculation loop, and ammonium oxalate crystal violet staining solution was added in a dropwise fashion to the smeared area, which was then stained for 1 min and washed with water. After blotting with absorbent paper, anhydrous ethanol was also added in a dropwise fashion to cover the entire smear area and then washed with water for 30 s. After blotting with absorbent paper, safranin dye solution was added in a dropwise fashion and stained for 1 min. The samples were then washed with water, blot dried with absorbent paper, and placed under a light microscope to observe bacterial morphology and Gram staining. Afterward, 100 mL of bacterial liquid cultured to the logarithmic phase was centrifuged at high speed at 4 °C, fixed with 2.5% glutaraldehyde overnight, and centrifuged to store the bacteria. The bacteria were subjected to gradient dehydration with 30%, 50%, 75%, 90%, and 100% ethanol (10 min per step). The samples were then freeze-dried at −20, −40, −60, and −80 °C and kept at each temperature for 12 h. After sample loading and gold spraying, the samples were examined via scanning electron microscopy (Regulus 8100, Hitachi High-Tech, Tokyo, Japan). Next, 20 μL of resuspended samples were placed dropwise on 200-mesh grids and incubated at room temperature for 10 min. Then, the cell morphology was examined using a transmission electron microscope (HT7700, Hitachi High-Tech, Tokyo, Japan).

Bacterial cultures in the logarithmic phase were frozen and centrifuged to obtain the bacterial cells for DNA purification and taxonomic classification based on 16S rRNA gene sequences. The extracted sample DNA was amplified by 16S rRNA, and PCR amplification was performed using a PCR instrument (2720 PCR instrument) with the 27F (5′- AGA GTT TGA TCC TGG CTC AG-3′) and 1492R (5′-GGT TAC CTT GTT ACG ACT G-3′) primer pair. The PCR amplification reaction system (30 μL) included 2 X EasyTaq SuperMix (15.0 μL), 27F (1μL), 1492R (1μL), DNA (1–2 μL), and $ddH_2O$ (up to 30 μL). The amplification consisted of a pre-denaturation step at 94 °C for 5 min, 25 cycles (denaturation at 94 °C for 30 s, annealing at 57 °C for 30 s, extension at 72 °C for 90 s), extension at 72 °C for 7 min, and storage at 4 °C. The amplicons were sequenced with a 3730 sequencer for the first generation of double-ended sequencing to obtain an ABI sequencing peak map file. After assembly, the sequence was compared with the 16s sub-library to identify closely related species. Upon comparing the 16S rRNA sequences in the NCBI database, the 19 strains that were closest to the species level were selected and the NJ (Neighbor-Joining) method was used to construct a phylogenetic tree using the MEGA 6.0 software to visualize the evolutionary relationship of the sample and the near-source species.

The bacteria obtained in the experiment were identified as pure *A. ferrooxidans*, after which their growth conditions were studied, including the optimum growth pH, temperature, and inoculum size. The cells were cultured in growth media at different pH conditions (pH 1.2, 1.8, 2.4, 3.0, 3.6, and 4.2) to explore the optimal pH conditions for bacterial growth. The cells were cultured at 15, 20, 25, 30, 35, and 40 °C to study the optimal

growth temperature. Finally, the cultures were inoculated with 5%, 10%, 15%, and 20% of the inoculum to explore the optimal inoculum amount. A blood cell counting plate was used to observe and calculate the bacterial concentration.

### *2.2. Whole genome Sequencing*

The bacteria collected above were sent to Beijing BMK Biological Co., Ltd., and whole genome sequencing was carried out using PacBio sequencing technology. The experimental process was performed according to the standard protocol provided by PacBio [12], including sample quality detection, library construction, library quality detection, and library sequencing. Low-quality and short fragments with a length of less than 2000 bp were removed from the reads obtained after sequencing, and clean reads were obtained for genome assembly and functional annotation. To fully display the features of the genome, a genome circle diagram of a single sample was generated using the Circos software (Version 0.69-6, http://www.circos.ca (accessed on 4 January 2023)) and a variety of information was displayed in the diagram to provide a comprehensive and intuitive understanding of the characteristics of the bacterial genome. Chromosome genes were predicted using Glimmer and the plasma genome was predicted using GeneMarkS [13,14]. The predicted genome was compared with the COG and KEGG databases based on protein sequence, and functional annotation was performed to obtain the corresponding gene function information. Upon sequencing the whole genome of *A. ferrooxidans* YQ-N3, short-length circular consensus sequencing (ccs) reads were filtered out from the raw data as a quality control measure. The filtered ccs reads were assembled de novo, and the assembled genome was corrected for errors. Once the assembly was completed, genome analysis and functional annotation were performed. Mobile genetic elements (MGEs) can help bacteria overcome challenges or occupy dominant niches. Therefore, studying the MGEs in the *A. ferrooxidans* YQ-N3 genome could provide insights into their ability to adapt to environmental changes. In this study, we analyzed three types of MGEs: genome islands, prophages, and CRISPR (clustered regularly interspersed short palindromic repeats)-Cas. Gene island prediction of the *A. ferrooxidans* YQ-N3 genome was performed using Islander (Version 1.2, http://www.pathogenomics.sfu.ca/islandviewer/ (accessed on 4 January 2023)) [15]. Prophage prediction was performed using Phage_Finder (phage-finder.sourceforge.net) [16]. CRISPR-Cas prediction was performed using Minced [17].

### *2.3. Comparative Genomic Analysis*

To further examine the genomic characteristics of *A. ferrooxidans* YQ-N3, the genomes of five strains closest to it at the species level based on 16S rRNA sequences were selected for comparative analysis. The genome sequences of the selected strains (*A. ferrooxidans* ATCC23270, *A. ferrooxidans* BY0502, *A. ferridurans* JCM18981, *A. thiooxidans* ATCC 19377, and *A. ferrivorans* SS3) were obtained from the GenBank database. Glimmer 3.0 (http://ccb.jhu.edu/software/glimmer/index.shtml (accessed on 4 January 2023)) and GeneMarkS (Predictive Plasmid Genome) software (Version 4.3, http://topaz.gatech.edu/GeneMark (accessed on 4 January 2023)) were used to predict the coding sequence (CDS) of genome. The core gene and pan-genome in the predicted sequence were analyzed using BPGA (Bacterial Pan-genome Analysis tool ver. 1.2, https://iicb.res.in/bpga/index.html (accessed on 4 January 2023)). The empirical power law equation and exponential equation were used to calculate the extrapolation of the pan-genome and core genome curves, respectively [18,19]. ANI analysis of the selected genome was conducted by using the pyani software following the ANIm method. AAI analysis of the selected genome was performed using the CompareM software (https://github.com/dparks1134/CompareM (accessed on 4 January 2023)). Genome alignments between *A. ferrooxidans* YQ-N3 and *A. ferrooxidans* ATCC23270, *A. ferrooxidans* BY0502, *A. ferridurans* JCM18981, *A. thiooxidans* ATCC 19377, and *A. ferrivorans* SS3 were conducted using the MUMmer software (ver. 3.23, https://sourceforge.net/projects/mummer/files/latest/download (accessed on 4 January 2023)) related to the ucmer comparison method. Based on protein sequence

alignments, the coding genes predicted on the *A. ferrooxidans* YQ-N3 and the genome of the other five studied strains were compared with the COG (clusters of orthologous groups of proteins) databases for functional annotation, and the corresponding functional annotations were obtained.

### 2.4. Oxidation Characteristics of $Fe^{2+}$, $S^0$, and $FeS_2$

As the dominant microbe in metallic sulfide mining areas, *A. ferrooxidans* plays a vital role in Fe and S biogeochemical cycling [20]. Therefore, studies on the $Fe^{2+}$, $S^0$, and $FeS_2$ oxidation capacities of novel *A. ferrooxidans* strains are essential, specifically due to their theoretical and practical values.

This study characterized the *A. ferrooxidans* strain YQ-N3 isolated in the previous stage, and its ability to oxidize $FeSO_4 \cdot 7H_2O$, $S^0$, and $FeS_2$ as energy sources was discussed. The preserved YQ-N3 strain was transferred to 9K medium containing $FeSO_4 \cdot 7H_2O$, $S^0$, and $FeS_2$ with 10% of the inoculum, and was then placed in a constant temperature culture shaker at 30 °C and 180 r/min for multiple activations. The bacterial density was determined using a hemocytometer, after which acclimated log-phase bacteria were collected. The domesticated strains were inoculated into 9K medium containing $FeSO_4 \cdot 7H_2O$, $S^0$, and $FeS_2$ at a 10% inoculum volume proportion, and the bacterial concentration and $Fe^{2+}$, $Fe^{3+}$, $SO_4^{2-}$, pH, and Eh in the culture system were monitored thereafter. The specific experimental design is shown in Table 1. Three parallel groups and one blank control were set for each group of experiments.

**Table 1.** Study design for the assessment of $Fe^{2+}$, $S^0$, and $FeS_2$ oxidation using *A. ferrooxidans* YQ-N3.

| Group | Energy Source | Bacterial Inoculum |
|---|---|---|
| *A.f* Oxidation $Fe^{2+}$ | $FeSO_4 \cdot 7H_2O$ (8.95 g) | 10% |
| Control 1 | $FeSO_4 \cdot 7H_2O$ (8.95 g) | 0% |
| *A.f* Oxidation $S^0$ | $S^0$ (0.5 g) | 10% |
| Control 2 | $S^0$ (0.5 g) | 0% |
| *A.f* Oxidation $FeS_2$ | $FeS_2$ (5 g) | 10% |
| Control 3 | $FeS_2$ (5 g) | 0% |

All experiments were conducted with 200 mL of 9K medium without Fe.

At the end of the experiment, mineral samples generated via the oxidation of $Fe^{2+}$ and $FeS_2$ before and after the reaction were collected. The samples were then ground and screened for mineral composition analysis. The phases and components of the collected samples were determined via X-ray diffraction (XRD) using an X-ray diffractometer (Bruker D8 ADVANCE, Karlsruhe, Germany) with Cu Kα radiation operating at 40 kV and 30 mA. The samples were scanned at a 0.02 °/s rate to record the patterns within a 2θ range of 3–105°; the mineral composition of the sample was then analyzed.

### 2.5. Coal Biodesulfurization Experiment

To explore the applicability of *A. ferrooxidans* YQ-N3 in coal desulfurization, three coal samples with different sulfur content from different mining areas in China were selected to conduct biological desulfurization experiments. The sulfur contents of the coal samples are shown in Table 2. The coal desulfurization experiments were conducted using a sequential batch experiment approach. Each coal sample was set with six groups of experiments, which included three replicates and one blank. Coal samples were taken at 5, 10, 15, 20, 25, and 30 days, respectively, to detect the sulfur contents. The experiment was carried out in 250 mL conical flasks in a constant temperature culture shaker at 30 °C and 180 r/min. All conical flasks contained 90 mL 9K liquid medium (free $Fe^{2+}$), 5 g of coal sample powder (200 mesh), and 10 mL of *A. ferrooxidans* YQ-N3 bacterial solution ($2.0 \times 10^7$ cells/mL). The initial pH of all growth media was adjusted to 2. The total sulfur and sulfur contents of coal samples were analyzed according to the national standards (GB/T214-1996 and GB/T215-1996) of China.

**Table 2.** Sulfur contents of coal samples.

| Coal Samples | Total S | $S_p$, Ad | $S_o$, Ad | $S_s$, Ad |
|---|---|---|---|---|
| I | 3.46% | 1.02% | 0.81% | 1.63% |
| II | 3.02% | 1.27% | 0.83% | 0.92% |
| III | 2.77% | 0.83% | 1.42% | 0.52% |

$S_p$, ad: sulfur in the form of pyrite; $S_o$, ad: sulfur in organic form; $S_s$, ad: sulfur in the form of sulfate.

## 3. Results and Discussion

### *3.1. Growth Characteristics of A. ferrooxidans YQ-N3*

In this study, sediment was collected from a river polluted by AMD of an abandoned mine in Shanxi, China. The sediment samples were treated with sterile water and inoculated in 9K-$Fe^{2+}$ liquid medium for enrichment culture. After cultivation, all three replicate cultures exhibited the same characteristics. The color of the medium gradually changed from light blue–green to turbid, after which it became clear red–brown after continued cultivation. After culturing on 9K-$Fe^{2+}$ solid medium for 30 days via the dilution coating method, colonies appeared on the plate, as illustrated in Figure 1A. The colonies were round, with prominent centers, neat edges, and yellow surroundings. After repeated solid–liquid alternating culture, the bacteria were collected, and DNA was extracted for 16S rRNA gene amplification and sequencing. After gene amplification, there was a single clear target band, which has 99.93% similarity with *Acidithiobacillus ferrooxidans* (NR_074193.1) according to the comparison between the sequencing results and BLAST. Therefore, the bacterial strain was named *A. ferrooxidans* YQ-N3. The collected bacteria were diluted several times using normal saline and then observed via Gram staining, thus confirming that the bacteria were Gram-negative. Optical microscope observations showed that the bacteria were rod-shaped (both as single cells and aggregates) and were able to swim rapidly. SEM and TEM analyses indicated that the bacteria had a short rod shape with blunt rounded ends, as shown in Figure 1B,C, with a length of approximately 0.8–1.2 μm and a width of 0.2–0.5 μm.

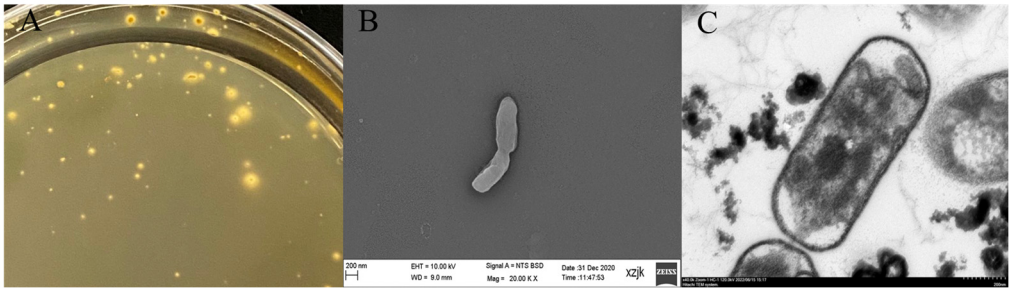


**Figure 1.** Phenotypic features of the new isolated *A. ferrooxidans* YQ-N3. ((**A**) is colonies on the plate; (**B**) is morphology of *A. ferrooxidans* YQ-N3 under SEM; (**C**) is morphology of *A. ferrooxidans* YQ-N3 under TEM.).

Upon comparing the 16S rRNA sequences in the GenBank database, the 18 strains that were closest at the species level were selected, and the NJ method was used to construct the phylogenetic tree of *A. ferrooxidans* YQ-N3 using the MEGA 6.0 software, as shown in Figure 2. The phylogenetic tree analyses demonstrated that *A. ferrooxidans* YQ-N3 was distinct from *Pseudomonas*, *Oceanicoccus*, *Luteimonas*, and *Xanthomonas*, but appeared to be related to *A. thiooxidans*, *A. ferridurans*, and *A. ferrivorans*. Particularly, the 16S rDNA sequence of *A. ferrooxidans* YQ-N3 was more than 99.93% similar to that of *A. ferrooxidans* ATCC23270, and it was therefore concluded that the isolated strains were *A. ferrooxidans*.

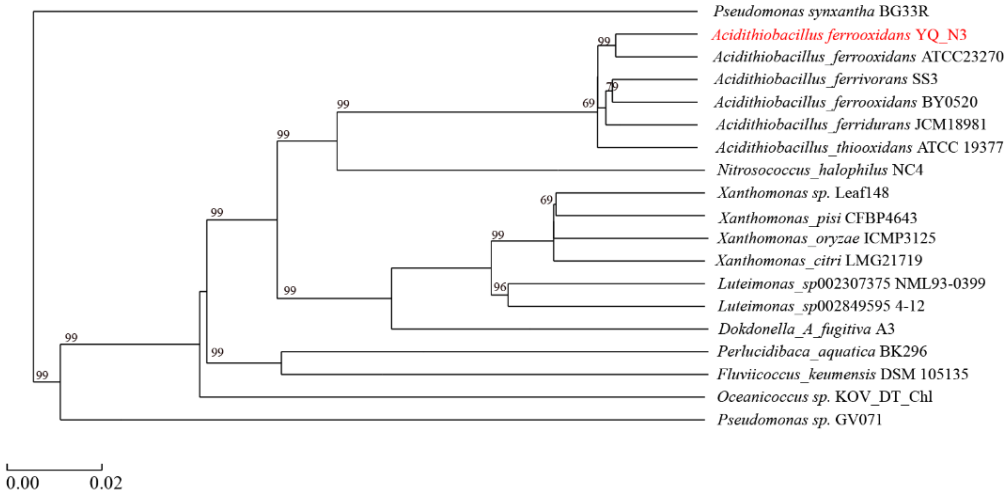


**Figure 2.** Phylogenetic tree of *A. ferrooxidans* YQ-N3 sequences and other sequences obtained from the GenBank database.

After screening and obtaining pure *A. ferrooxidans* YQ-N3 cultures, the optimum growth conditions were explored. Our findings demonstrated that *A. ferrooxidans* YQ-N3 could grow at a pH range of 1.6–2.4 and a temperature range of 20–35 °C, and were therefore consistent with previous studies. The strain achieved optimal growth at an initial pH of 1.8, a temperature of 30 °C, and an inoculum volume of 10%. Under these conditions, *A. ferrooxidans* YQ-N3 could reach a density of up to $2.3 \times 10^8$ cells/mL after 16 h.

### *3.2. Genome Overview of A. ferrooxidans YQ-N3*

Whole genome analysis indicated that the genome size of *A. ferrooxidans* YQ-N3 was 3,217,720 bp, including one circular chromosome and five circular plasmids (Plasmid A, Plasmid B, Plasmid C, Plasmid D, and Plasmid E). The sequence length of the circular chromosome was 3,043,496 bp and the GC content was 58.64%. To fully demonstrate the genome features of *A. ferrooxidans* YQ-N3, a genome circle plot was drawn using the Circos software (Figure 3). A total of 3200 coding sequences (CDs), 6 rRNAs, 46 tRNAs, and 18 sRNAs were predicted. The annotation results of plasmids are shown in Table 3. The sequence length of the circular Plasmid A was 79,659 bp and the GC content was 61.64%. The length of Plasmid B was 34,460 bp and the GC content was 60.54%. The sequence length of Plasmid C was 29,178 bp and the GC content was 62.67%. The sequence length of Plasmid D was 23,017 bp and the GC content was 60.69%. The sequence length of Plasmid E was 7910 bp and the GC content was 52.40%. Among them, the Plasmid E sequence had not been annotated in the reference database. The complete genome sequences for the main chromosome and Plasmids A-E of *A. ferrooxidans* YQ-N3 were submitted to the GenBank database under accession numbers CP084172.1, CP084173.1, CP084174.1, CP084175.1, CP084176.1, and CP084177.1, respectively. *A. ferrooxidans* can grow in a variety of extreme environments and has great potential applications in industries such as bioleaching and biological desulfurization [21–23]. However, there are 26 published genomes of *A. ferrooxidans* strains, and therefore the whole genome sequencing and analysis of *A. ferrooxidans* YQ-N3 could provide key insights into its genetic properties and potential applicability. To understand the differences between the genomes of *A. ferrooxidans* YQ-N3 and other *A. ferrooxidans* strains, the genome information of *A. ferrooxidans* YQ-N3 and *A. ferrooxidans* that has been published in GenBank was selected for tabulation analysis, as shown in Supplementary Materials Table S1. The genome size distribution of *A. ferrooxidans* was 2.82631–4.18422 Mb, the GC content was 56.8%–58.9%, and the CDS (coding sequence) distribution was 2705–3998. The genome size, GC%, and number of CDSs of *A. ferrooxidans* YQ-N3 are similar to those of other *A. ferrooxidans* strains. However, with the exception

of *A. ferrooxidans* YQ-N3, the assembled *A. ferrooxidans* genome in the published database included no more than five plasmids.

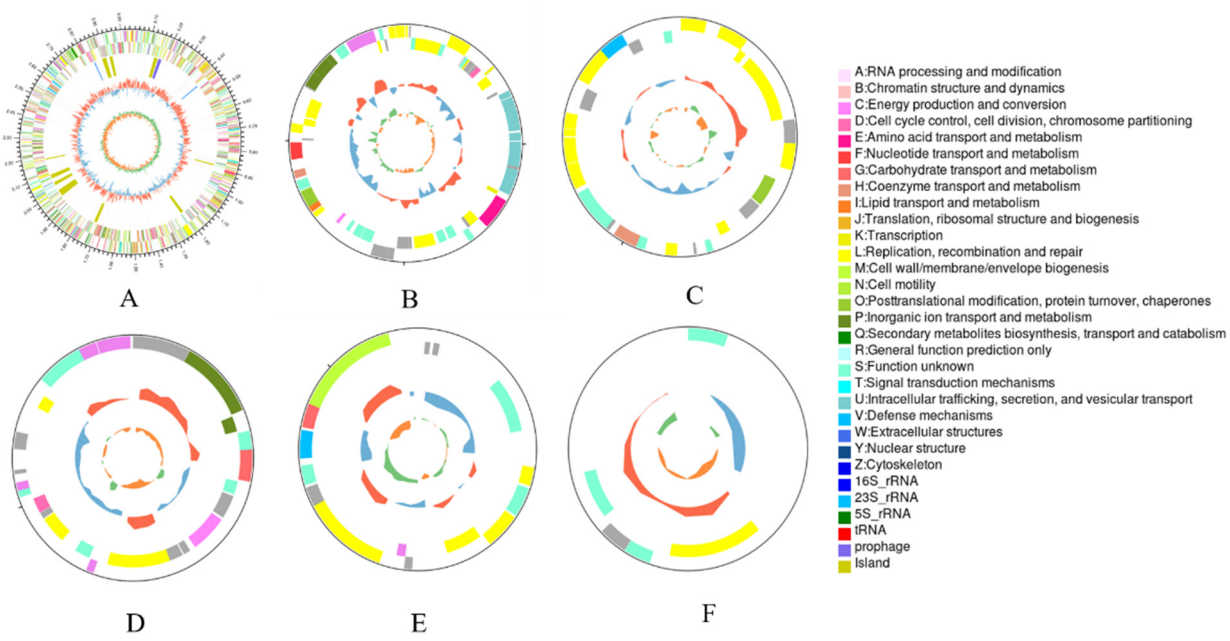


**Figure 3.** Circular genome map of *A. ferrooxidans* YQ-N3. From outside to center: genes on the direct strand, genes on the complementary strand, tRNAs (orange), rRNA (purple), CRISPR (blue), and genomic island (green). GC-skew and sequencing depths are also displayed. (**A**) Chromosome, (**B**) Plasmid A, (**C**) Plasmid B, (**D**) Plasmid C, (**E**) Plasmid D, and (**F**) Plasmid E.

**Table 3.** Table of Plasmids' Annotation Details.

| Location | Sequence Length (Bp) | GC Content (%) | Accession Number | Accession Strain Name | Accession Plasmid Name | Identity (%) |
|---|---|---|---|---|---|---|
| Plasmid E | 7910 | 52.4 | - | - | - | - |
| Plasmid D | 23,017 | 60.69 | NC_015188.1 | *Acidiphilium multivorum* AIU301 | pACMV4 | 88.265 |
| Plasmid C | 29,178 | 62.67 | NC_015178.1 | *Acidiphilium multivorum* AIU301 | pACMV1 | 88.293 |
| Plasmid B | 34,460 | 60.54 | NC_009470.1 | *Acidiphilium cryptum* JF-5 | pACRY04 | 96.491 |
| Plasmid A | 79,659 | 61.64 | NC_009469.1 | *Acidiphilium cryptum* JF-5 | pACRY03 | 99.949 |

"-" indicates no data.

### 3.3. Comparative Genomic Analysis

A summary of the features of six selected genomes is listed in Table 4. These strains were collected from different environments around the world but mainly from acid mine drainage. These genomes vary in size by approximately 0.44 Mb (ranging from 2.98 to 3.42 Mb) with coding sequence (CDS) numbers ranging from 2927 to 3498 and the G+C contents of the genomes ranging from 53% to 58.8%. Figure 4 shows the results of ANI and AAI analysis among strains. The squares with different colors show the similarity of nucleotides and amino acids among stains. It can be seen that *A. ferrooxidans* YQ-N3 is closely related to *A. ferrooxidans* ATCC23270 and *A. ferridurans* JCM18981. The ANI value and AAI value between *A. ferrooxidans* YQ-N3 and *A. ferrooxidans* ATCC23270 exceeded 95%, indicating that *A. ferrooxidans* YQ-N3 and *A. ferrooxidans* ATCC23270 are the same species. The results of the whole genome alignment between *A. ferrooxidans* YQ-N3 and the selected genomes are shown in Figure 5. Our findings indicated that the genomic arrangement of *A. ferrooxidans* YQ-N3 has the best co-linearity with *A. ferrooxidans* ATCC23270, and has better co-linearity with *A. ferridurans* JCM18981 than with *A. ferrooxidans* BY0502. This result demonstrates that *A. ferrooxidans* YQ-N3 and *A. ferrooxidans* ATCC23270 have closer evolutionary distances and highlights the abundant evolutionary progress of *A. ferrooxidans*.

**Table 4.** General features of bacterial genomes used in this study.

| Strain | Geographic Origin | Genome Size (Mb) | GC% | Level | CDS | Genes |
|---|---|---|---|---|---|---|
| *A. ferrooxidans* YQ-N3 | Shanxi, China | 3.22 | 58.7 | Complete | 3195 | 3252 |
| *A. ferrooxidans* ATCC23270 | Bituminous coal mine effluent | 2.98 | 58.8 | Complete | 2927 | 3087 |
| *A. ferrooxidans* BY0502 | Gansu, China | 2.98 | 56.8 | Contig | 3026 | 3186 |
| *A. ferridurans JCM18981* | Okayama, Japan | 2.98 | 58.4 | Complete | 2802 | 3043 |
| *A. thiooxidans* ATCC 19377 | - | 3.42 | 53 | Contig | 3498 | 3584 |
| *A. ferrivorans SS3* | Norilsk, Russia | 3.20 | 56.5 | Complete | 3089 | 3200 |

"-" indicates no data.

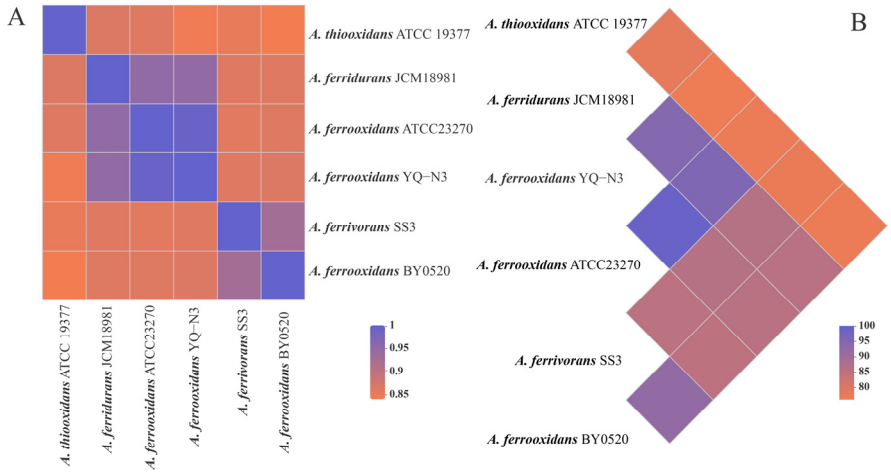


**Figure 4.** Strain ANI matrix thermogram (**A**) and strain AAI triangle thermogram (**B**).

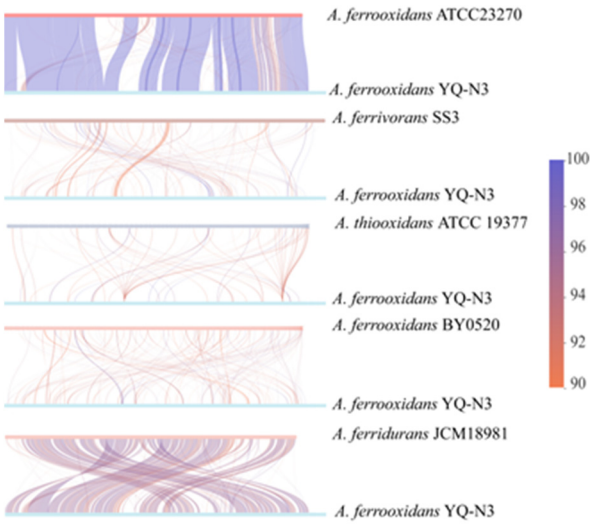


**Figure 5.** Whole genome alignment between *A. ferrooxidans* YQ-N3 and the selected genomes.

The bacterial pan-genome (BGPA) was used to identify orthologous groups among the studied genomes to reveal the unique genomic characteristics of the studied strains. The results are shown in Figure 6. The pan-genome contains 6062 genes, including 1400 core genomes and 2918 unique genomes. Figure 6B shows the curve of the relationship between the pan-genome size, core genome size, and genome number. According to the formula of the relationship curve between the pan-genome size and genome number ($f(n) = 2239.763n^{0.497} + 580.101$), we can conclude that the pan-genome in this study is open-type ($0 < 0.497 < 1$) [24], which means that as the number of sequenced genomes continues to increase, the pan-genome size will increase indefinitely. The core genome is composed of

genes that exist in all strains and is generally related to the basic biological functions and main phenotypic characteristics of bacteria. The unique genome is composed of genes only existing in some strains and genes unique to a strain, which reflects the diversity of strains and is generally related to some special biological metabolic pathways and environmental adaptation, such as antibiotic production, tolerance, and virulence. The rich specific genome content in this study indicates that the studied strains may undergo horizontal gene transfer (HGT) to improve their own survival competitiveness and increase microbial diversity [25].

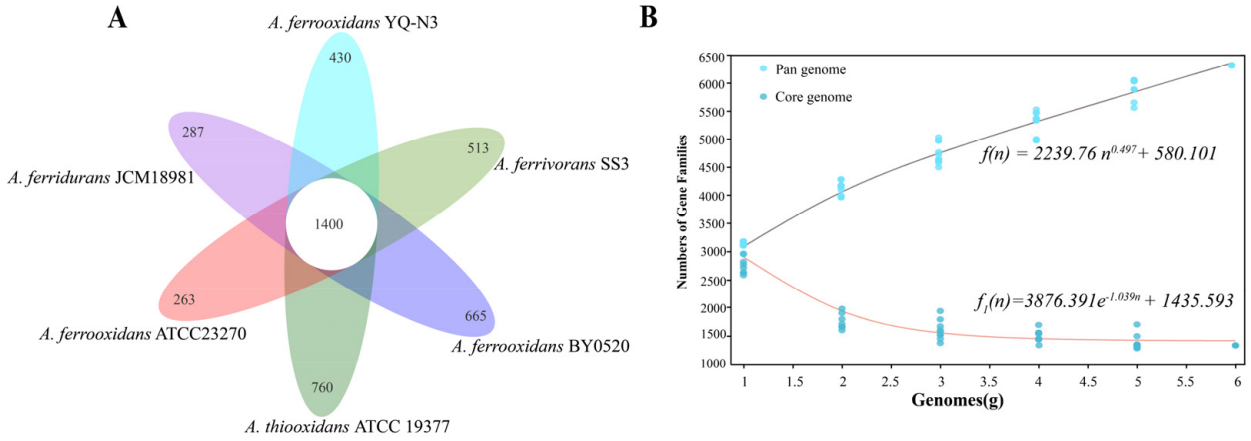


**Figure 6.** Pan-genome analysis of strains in this study. (**A**) Venn diagram of the pan-genome; (**B**) mathematical modeling of the pan-genome and core genome of strains in this study.

Figure 7 shows the COG annotation category and function statistics of the studied strains. These COGs were divided into four categories and 24 functional classes. The proportion of genes related to replication, recombination, and repair (L), cell wall/membrane/envelope biogenesis (M), energy production and conversion (C), and inorganic ion transport and metabolism (P) was slightly higher than that of genes with other functions, accounting for 5.55%–7.18%, 8.16%–9.71%, 6.66%–7.58%, and 5.55%–6.89% of all annotated genes, respectively. Additionally, defense mechanisms accounted for 4.92%–5.91% of all annotated genes, suggesting that these strains have a strong ability to self-repair and resist harsh environments [1]. *A. ferrooxidans* YQ-N3 has a total of 2571 genes annotated in COG, accounting for approximately 80.34% of the total number of genes. Compared to other strains, *A. ferrooxidans* YQ-N3 had the most genes associated with functions supporting P, L, and J (translation, ribosomal structure, and biogenesis). Moreover, the distribution of functional genes in the *A. ferrooxidans* YQ-N3, *A. ferrooxidans* ATCC23270, and *A. ferrooxidans* BY0502 genomes showed a similar pattern.

*A. ferrooxidans* is widely found in metal mines, high-sulfate coal mines, and other extreme environments due to its high environmental resistance, as well as its tolerance to metal ions and high acidity [26]. The characterization of genes associated with environmental resistance in *A. ferrooxidans* YQ-N3 would provide insights into the mechanisms that mediate its adaptability, which also lays the foundation for future research on its survival state and industrial application value in extreme environments. The results of COG annotation showed that the YQ-N3-gene-1491 and YQ-N3-gene-2286 located in the chromosome were annotated as ENOG410ZI6F and their COG description was "heavy metal transport detoxification protein", which further suggested that this strain was resistant to heavy metals. Some metal resistance genes have also been found, such as cusA, cusB, cusR, and cusS. Previous studies have demonstrated that the cus proton pump system is widely distributed in Gram-negative bacteria and is associated with copper and silver resistance in *A. ferrooxidans* [27]. In fact, cusA, cusB, and cusF possess metal-binding sites, and $Cu^{2+}$ is directly transferred from protein to protein in the cus system during ion transport, thereby reducing the potential toxicity of free $Cu^{2+}$ to cells [28,29]. Nan et al. linked the adaptability

of *A. ferrooxidans* to chemotactic movement and quorum sensing (QS), both of which allow this bacterium to grow, develop, and reproduce in extreme environments [30].

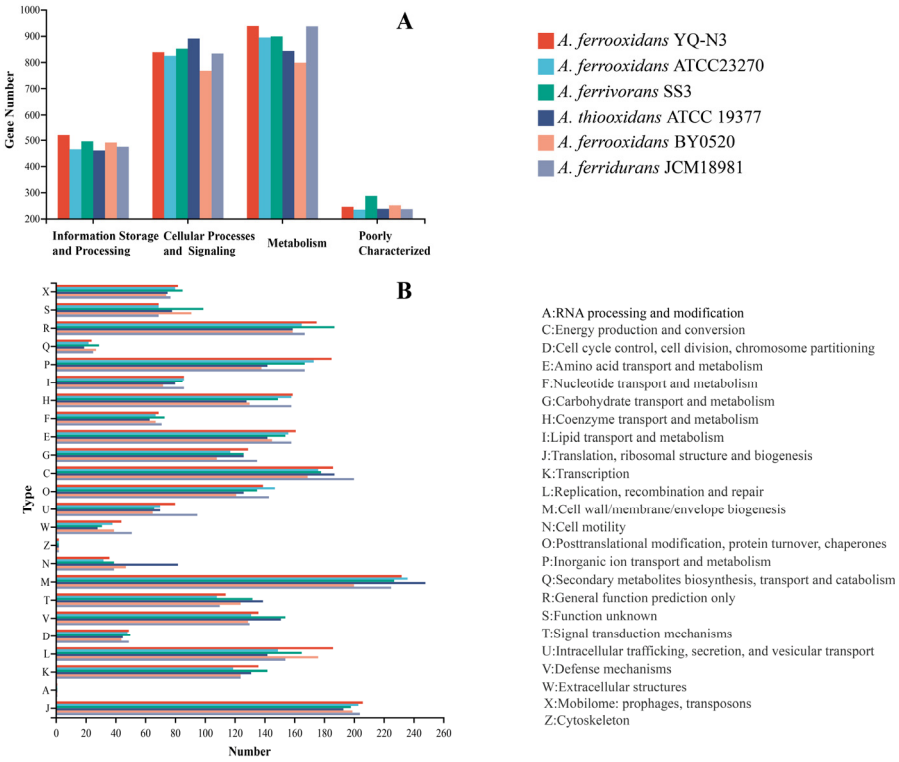


**Figure 7.** Comparison of COG categories (**A**) and COG functions (**B**) of strains in this study.

### *3.4. MEGs*

More than 20% of genes in microbial genomes may be obtained through horizontal gene transfer (HGT), and these genes are usually referred to as mobile genetic elements (MGEs) [31,32]. MGEs refer to some exogenous gene fragments by way of the HGT that can be incorporated into bacterial genomes to adapt to environmental changes or improve the likelihood of survival. These fragments generally contain genes that encode the enzymes of other proteins with specific functions to help bacteria overcome adverse conditions or take advantage of resources that otherwise could not be exploited. The gene islands often carry functional genes, contain integrase and plasmid conjugation-related factors [33]. The prophage sequence often contained some functional genes, such as antibiotic resistance genes and virulence genes, among others, all of which enhanced the adaptability of this bacterium to its environment [34]. The CRISPR/Cas system is a prokaryotic immune system designed to resist the invasion of exogenous genetic material [35]. Integrators can enhance the adaptability of bacteria by capturing exogenous genes. Some studies have indicated that HGT is the main mechanism for acidophilic bacteria to adapt to heavy metal-rich environments [36–38]. The research on MGEs is helpful to further explore the whole genome characteristics of species. In this study, we analyzed the MGEs of *A. ferrooxidans* YQ-N3 from phages, genomic islands (GIs), and integrons. The predicted results indicated that the chromosome of *A. ferrooxidans* YQ-N3 contained 10 gene islands and Plasmid A contained one gene island. In turn, these gene islands contained a total of 181 CDs. The linear map of genome islands is shown in Figure 8. The description of genes 1255, 1259, 1624, 1270, and 1274 are "DEAD/DEAH box helicase", "hypothetical protein", "phage anti-repressor Ant", "M48 family metalloprotease", and "MULTISPECIES: restriction endonuclease", respectively. Interestingly, our analyses indicated that a prophage genome had integrated into the chromosome of *A. ferrooxidans* YQ-N3. The sequence length of the prophage was 17,089 bp and had 19 CDs, in addition to having a 58.64% GC content. The chromosome of *A. ferrooxidans* YQ-N3 was predicted to contain four CRISPRs with

average repeat lengths of 27, 28, 23, and 27 bp, respectively. The average lengths of the spacer sequences were 27, 32, 43, and 45 bp, respectively. An integron was also found on a chromosome of *A. ferrooxidans* YQ-N3. Its structure is shown in Figure 9; its length was 123 bp, including 9 CDs. Therefore, from the perspective of the whole genome, *A. ferrooxidans* YQ-N3 is likely resistant to heavy metals and is highly adaptable, making it a promising candidate for various industrial applications such as biological desulfurization, bioleaching, metal processing, and others.

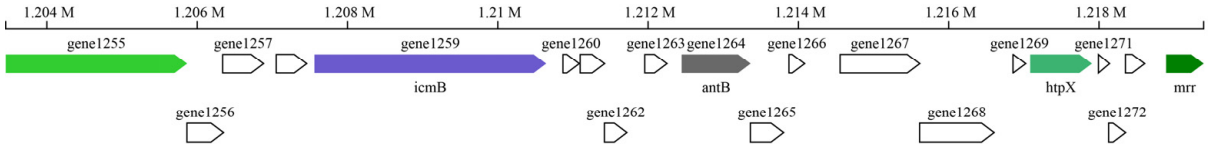


**Figure 8.** Linear map of genome islands. (The arrows represent genes, the length of the arrow represents the gene length, the direction indicates that the gene is encoded by a sense chain or antisense chain, and the color represents its COG function classification. The arrow without color represents that the corresponding COG function is not annotated. COG function classifications of gene 1252, gene 1259, gene 1264, htpX and mrr are type L, type S, type K, type O and type V).

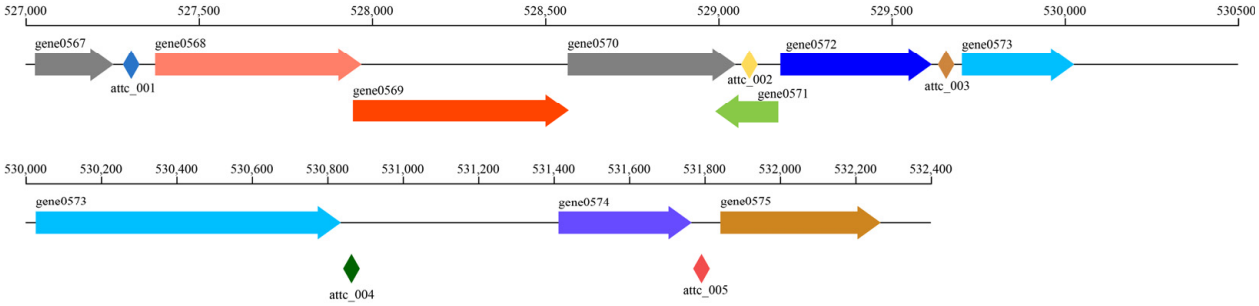


**Figure 9.** Integron structure diagram (attC is the recombination site necessary for integration).

### *3.5. Genes Associated with Iron and Sulfur Metabolism*

To further understand the whole genome characteristics of *A. ferrooxidans* YQ-N3, its genes related to iron and sulfur metabolism were deeply explored from a functional gene perspective. According to the KEGG annotation results of *A. ferrooxidans* YQ-N3, the genes related to iron and sulfur metabolism are summarized in Table S2. Our findings demonstrated that this strain possesses multiple genes related to $Fe^{2+}$ oxidation metabolism and sulfur metabolism. For example, cyc2, cyc1, coxB, coxA, and coxC, which encode the Rus operon components, were identified in *A. ferrooxidans* YQ-N3. Moreover, hdrB, hdrA, hdrC, tusA, and dsrE, which encode the HdrABC (isodisulfide reductase complex), were also detected. *A. ferrooxidans* is a chemoautotrophic bacterium with a complex energy metabolism pathway, which obtains energy through the oxidation of $Fe^{2+}$ and reduction of sulfur compounds, and generates energy to sustain its growth by fixing carbon and nitrogen in the air [39,40]. The oxidative metabolism of ferrous and sulfur compounds by *A. ferrooxidans* makes this bacterium especially well suited to industrial applications [41]. Previous studies have demonstrated that $Fe^{2+}$ oxidation by *A. ferrooxidans* in the electron transport chain has two patterns, including the downhill potential gradient and the uphill potential gradient [42]. Most electrons generated via $Fe^{2+}$ oxidation pass along the downhill potential gradient. Specifically, electrons generated by $Fe^{2+}$ oxidation enter the cytoplasm from the outer cell membrane, then pass to the cytochrome protein cyc2, after which they are received by rus, a ceruloplasmin, and passed to cyc2, a cytochrome protein. Afterward, they are received by cytochrome oxidase aa3 and then passed to $O_2$, where they finally combine with protons to generate $H_2O$ [43]. In this process, the oxidation process of the rus operon plays a dominant role, and the rus operon is composed of multiple genes including cyc2, coxA, coxB, coxC, and rus [44]. Furthermore, studies on

the regulation of the expression of key rus operon genes in model microorganisms show that the expression of the rus operon is induced by $Fe^{2+}$ [45,46]. The sqr gene, which encodes the sulfide quinone reductase enzyme, has been previously identified in various *A. ferrooxidans* strains [47]. doxDA encoding thiosulfate quinone reductase was also identified in ATCC23270 and CCM4253. When elemental sulfur was used as an energy source, the transcription level of the heterodisulfide reductase (HdrABC) complex encoded by ten genes including hdrB, hdrA, hdrC2, tusA, and hdrB2 was significantly upregulated, indicating that this complex was related to sulfur metabolism in *A. ferrooxidans* [48]. The query of functional genes confirmed that *A. ferrooxidans* YQ-N3 can oxidize $Fe^{2+}$ and sulfur, but its metabolic pathways require being further explored.

### 3.6. Oxidation of $Fe^{2+}$, $S^0$, and Pyrite

During $Fe^{2+}$ oxidation by *A. ferrooxidans* YQ-N3, the color of the medium gradually shifted from clear light green to yellow–green at first. After 16 h, the medium completely changed to reddish–brown. Then, a yellow precipitate gradually appeared in the reaction system. The blank control group did not exhibit any obvious color change. Figure 10 shows the trends of pH, ORP, $Fe^{2+}$ content, and total iron content of the medium during $Fe^{2+}$ oxidation. According to Figure 10A, the pH in the experiment involving *A. ferrooxidans* YQ-N3 increased from 1.8 to 2.16 after 48 h, and then rapidly decreased to 1.7. ORP also increased throughout the experiment but this trend decelerated slightly after 48 h. In the blank control group, pH and ORP showed a slight upward trend throughout the experiment. This can be attributed to $H^+$ consumption by the oxidation of $Fe^{2+}$ into $Fe^{3+}$ [49]. $Fe^{3+}$, $SO_4^{2-}$, and other cations (e.g., $K^+$, $Na^+$, $NH_4^+$) begin to react as the $Fe^{3+}$ content increases, which results in the production of $H^+$ and the minerals jarosite ($KFe_3(SO_4)_2(OH)_6$) and ammoniojarosite ($(NH_4)_2Fe_6(SO_4)_4(OH)_{12}$) (Figure 11), which is consistent with previous studies [50]. Therefore, the pH rapidly decreased and the ORP increase rate slowed down in the later stage of the experimental group [51]. Figure 10B shows that the $Fe^{2+}$ content in the experiment involving *A. ferrooxidans* YQ-N3 continued to decrease rapidly and the $Fe^{2+}$ content reached 0 mg/L when the reaction reached 60 h. The total iron concentration decreased by approximately 2700 mg/L during the whole reaction period, whereas only 14.5% $Fe^{2+}$ was oxidized and the total iron concentration in the blank control group remained unchanged for 96 h. This can be attributed to the fact that *A. ferrooxidans* YQ-N3 accelerates the oxidation of $Fe^{2+}$, and the $Fe^{3+}$ generated by the reaction leads to a decrease in the total iron content in the liquid phase. $Fe^{2+}$ is naturally oxidized and generates free $Fe^{3+}$ in the blank control group during the reaction, and therefore the total iron content remained unchanged in the system.

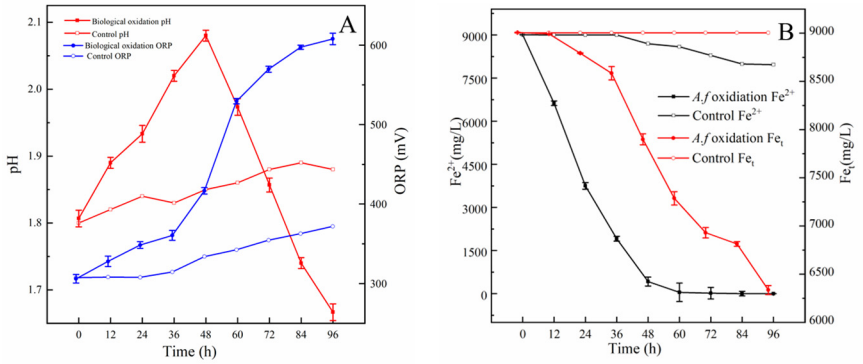


**Figure 10.** Trends of physicochemical indexes during $Fe^{2+}$ oxidation by *A. ferrooxidans* YQ-N3.((**A**) is the change of pH and ORP; (**B**) is the change of content $Fe^{2+}$ and total Fe. The error bar represents the standard deviation of three parallel experiments).

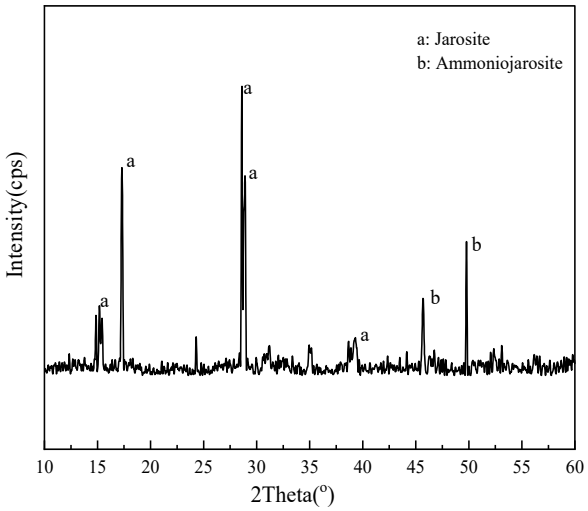


**Figure 11.** XRD pattern of minerals generated by $Fe^{2+}$ oxidated by *A. ferrooxidans* YQ-N3.

During the oxidation of $S^0$ by *A. ferrooxidans* YQ-N3, the medium gradually changed from clear and colorless to light yellow, the particle size of sulfur powder gradually became smaller, and its hydrophobicity gradually weakened. However, no obvious change was observed during the reaction of the blank control group. This phenomenon was mainly because *A. ferrooxidans* adsorbed on the surface of S when oxidizing it and secreted hydrophilic organic substances that covered the surface of S to enhance its hydrophilicity [52,53]. During the oxidation of $S^0$ by *A. ferrooxidans* YQ-N3, the pH value of the medium decreased from 2.2 to 1.74, whereas the $SO_4^{2-}$ concentration of the medium increased to 3896.66 mg/L after 45 d (Figure 12). This can be attributed to the release of $H^+$ through the oxidation of $S^0$ to $SO_4^{2-}$.

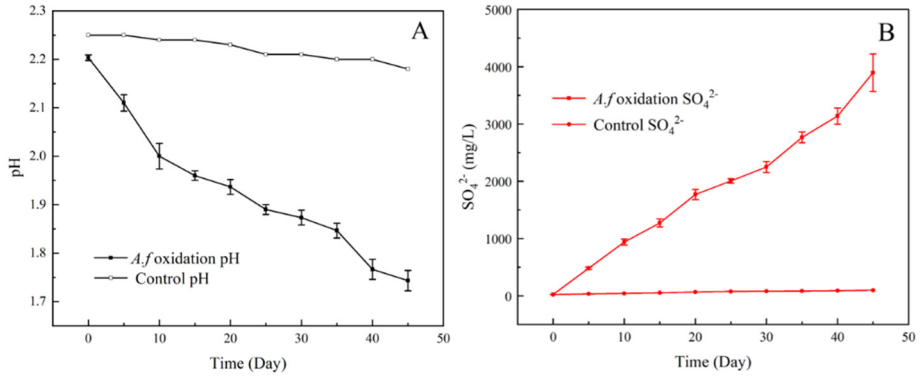


**Figure 12.** Trends of physicochemical indexes during $S^0$ oxidation by *A. ferrooxidans* YQ-N3. ((**A**) is the change of pH; (**B**) is the change of content $SO_4^{2-}$. The error bar represents the standard deviation of three parallel experiments).

Figure 13 illustrates the trends of pH, ORP, $SO_4^{2-}$, $Fe^{2+}$, and $Fe_t$ during pyrite oxidation by *A. ferrooxidans* YQ-N3. In the experimental group, the pH value decreased from 1.9 to 1.2 after 45 d, the ORP increased from 353 to 632 mV after 45 d, the $SO_4^{2-}$ concentration increased to 5433.8 mg/L after 45 d, the $Fe^{2+}$ content decreased drastically from 43.6 mg/L to a negligible level after 23 d, and the $Fe_t$ content increased to 3853 mg/L after 45 d. Characterization by XRD revealed that pyrite oxidized by *A. ferrooxidans* YQ-N3 contains jarosite and FeOOH, in addition to quartz impurities (Figure 14). In the blank control group, the pH value decreased slightly, the ORP decreased and then slightly increased, the $SO_4^{2-}$ concentration increased to 563 mg/L after 45 d, the $Fe^{2+}$ content increased to 178.2 mg/L after 45 d, and the $Fe_t$ concentration increased to 197.7 mg/L after 45 d. This could be because the $H^+$ released by the oxidation of $S^0$ into $SO_4^{2-}$ exceeded the levels

consumed by $Fe^{2+}$ oxidation. *A. ferrooxidans* YQ-N3 can accelerate the oxidation of $Fe^{2+}$ to $Fe^{3+}$ and pyrite oxidation can be carried out continuously and rapidly. The dissolved Fe mainly exists in the form of $Fe^{3+}$ in this system, and therefore ORP continues to increase.

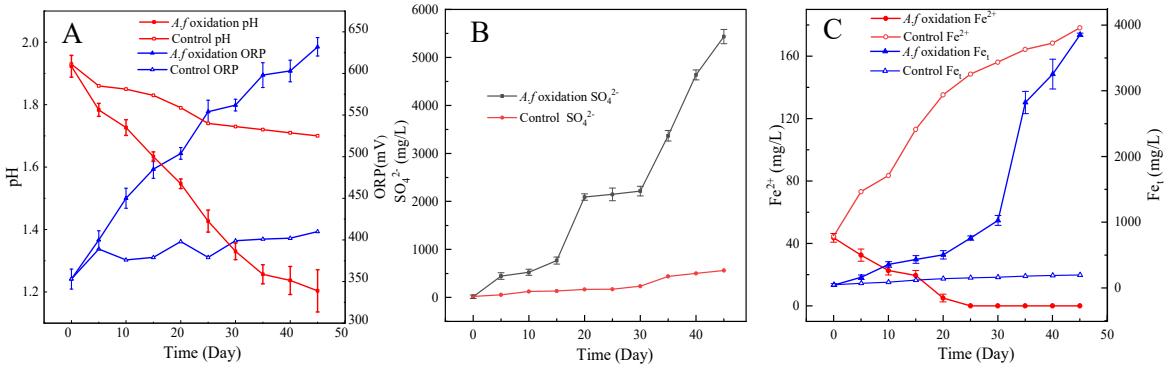


**Figure 13.** Trends of physicochemical indexes during $FeS_2$ oxidation by *A. ferrooxidans* YQ-N3. ((**A**) is the change of pH and ORP; (**B**) is the change of content $SO_4^{2-}$; (**C**) is the change of content $Fe^{2+}$ and total Fe. The error bar represents the standard deviation of three parallel experiments).

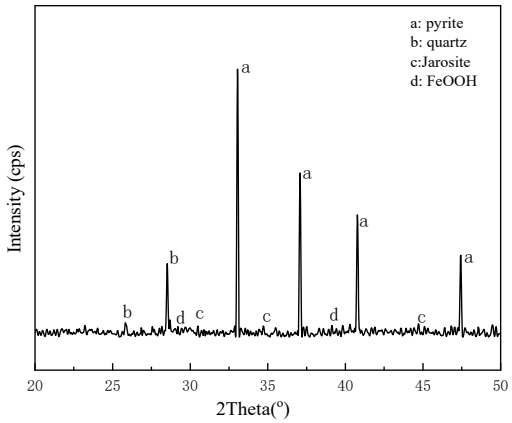


**Figure 14.** XRD pattern of residues after $FeS_2$ was oxidated by *A. ferrooxidans* YQ-N3.

The oxidation of different energy substances ($Fe^{2+}$, $S^0$, and pyrite) by *A. ferrooxidans* YQ-N3 was investigated via the shake bottle experiment. The results indicate that *A. ferrooxidans* YQ-N3 can accelerate the oxidation of $Fe^{2+}$ and that it contributes to the formation of minerals such as jarosite and ammoniojarosite while also accelerating the oxidation of $S^0$ and enhancing its hydrophilicity. *A. ferrooxidans* YQ-N3 can also achieve rapid and continuous oxidation of pyrite by accelerating $Fe^{2+}$ oxidation, thereby increasing the ORP. As a result, the pH value decreased, the $SO_4^{2-}$ concentration increased, and minerals (e.g., jarosite and FeOOH) were generated, all of which are hallmarks of the AMD generation process [54]. These findings suggest that *A. ferrooxidans* YQ-N3 can accelerate the production of AMD.

### *3.7. Desulfurization of Coal*

The direct combustion of coal can lead to a variety of environmental pollution problems. For example, the main reason for the formation of acid rain is the $SO_2$ gas released by the direct combustion of coal [55]. Therefore, it is particularly important to develop efficient desulfurization technology. The microbial desulfurization of coal not only promotes environmental protection but is also highly efficient and consumes few resources [56]. *A. ferrooxidans* is a commonly used coal desulfurization bacteria. Therefore, it is of great significance to study the coal desulfurization ability of *A. ferrooxidans* YQ-N3. The performance of *A. ferrooxidans* YQ-N3 during the coal desulfurization is illustrated in Figure 15.

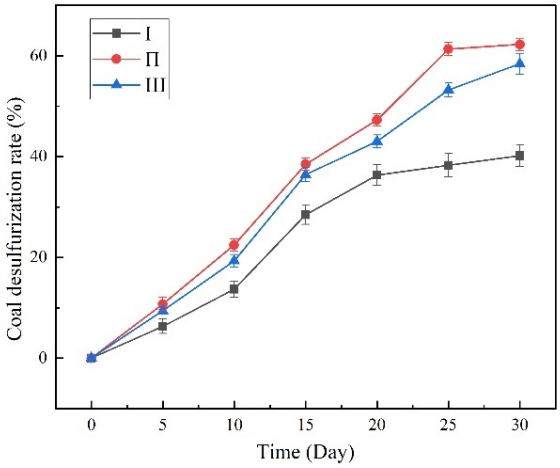


**Figure 15.** Sulfur removal efficiency during desulfurization.

During the desulfurization process, the sulfur removal rate of *A. ferrooxidans* YQ-N3 on the three coal samples continued to increase, and the sulfur removal rate of coal sample II was higher than that of coal samples III and I. After 30 days of reaction, the total sulfur removal rates of the I, II, and III coal samples were 40.17%, 62.25%, and 58.40%, respectively.

Table 5 shows the coal desulfurization characteristics of strain *A. ferrooxidans* YQ-N3 and other *A. ferrooxidans*. Our findings indicated that the coal desulfurization ability of *A. ferrooxidans* YQ-N3 was at a medium level. This may be due to the fact that the strain only grew in the ferrous environment and was not domesticated in any environment before the coal desulfurization experiments. Domesticated strains in specific environments (e.g., medium containing pyrite) and the optimization of desulfurization experimental parameters may improve the desulfurization capacity of *A. ferrooxidans* YQ-N3 [57].

**Table 5.** Main characteristics of different desulfurization strains.

| Strain | Geographic Origin | Highest Desulfurization Rate for Coal | Desulfurization Reaction Time | References |
|---|---|---|---|---|
| *A. ferrooxidans* YY2 | Guizhou, China | 75% | 30 days | [56] |
| *A. ferrooxidans* LY01 | Guizhou, China | 67.8% | 13 days | [57] |
| *A. ferrooxidans* | Johannesburg, South Africa | 79% | 14 days | [58] |
| *A. ferrooxidans* LX5 | China | 31.6% | 32 days | [59] |
| *A. ferrooxidans* DSM 583 | - | 30.84% | 12 h | [60] |
| *A. ferrooxidans* YQ-N3 | Shanxi, China | 62.25% | 30 days | This study |

"-" indicates no data.

Additionally, coal chemical analysis of coal samples after the desulfurization reaction was carried out. The results showed that the total sulfur content of I after the reaction was 2.07%, including 0.43% pyrite sulfur, 0.36% organic sulfur, and 1.28% sulfate sulfur. The total sulfur content of II was 1.14%, including 0.32% pyrite sulfur, 0.29% organic sulfur, and 0.53% sulfate sulfur. Coal sample III contains 1.165 total sulfur, 0.26% pyrite sulfur, 0.42% organic sulfur, and 0.48% sulfate sulfur. It can be seen that the sulfur removal rate for coal samples with high pyrite content (II) is higher than that for coal samples with high organic sulfur content (III), and higher than that for coal samples with high sulfate sulfur content (I). Some studies showed that the desulfurization capacity of *A. ferrooxidans* is mainly due to the ability of this bacterium to oxidize pyrite in coal [8]. The mechanisms through which *A. ferrooxidans* oxidizes the pyrite in coal can be divided into two modes: direct action and indirect action. The direct action mechanism refers to that during the oxidation of pyrite. Particularly, the bacteria uses the adhesion of fixed organs, pili, or mineral surfaces to directly adsorb on the pyrite surface. Pyrite is directly decomposed

into ferrous ions and sulfur through protein secretion or other metabolites (ferrous oxidase, cytochrome C oxidase, cytochrome oxidoreductase, etc.), and sulfur is further oxidized to $SO_4^{2-}$ by *A. ferrooxidans* [58,61]. Indirect action means that although *A. ferrooxidans* cells adsorb on the surface of minerals, they do not directly oxidize pyrite, but oxidize $Fe^{2+}$ to $Fe^{3+}$ in solution. $Fe^{3+}$ has a strong oxidation ability to oxidize pyrite to release $Fe^{2+}$ and generate $H^+$ and $SO_4^{2-}$. $Fe^{2+}$ is further oxidized in solution to generate $Fe^{3+}$. This process is repeated to continuously remove pyrite from coal [62]. The organic sulfur compounds of coal exist in the form of thiols, mercaptans, sulfide, and disulfide linkages, as well as complex thiophene moieties. Organic sulfur is considered more recalcitrant compared to its inorganic counterparts. Rout et al. reported that the microbial desulfurization process assisted by *A. ferrooxidans* successfully resulted in the removal of 84.75% of organic sulfur from coal samples. The authors also reported that *A. ferrooxidans* performed oxidative desulfurization of the model sulfur-containing organic compound dibenzothiophene to 2-hydroxy biphenyl through the formation of dioxy-dibenzothiophene [9,63]. Therefore, the results of this study have demonstrated that *A. ferrooxidans* YQ-N3 cells are capable of biological desulfurization. Therefore, these cells can be used to oxidize pyrite sulfur and organic sulfur in coal.

## 4. Conclusions

A novel *A. ferrooxidans* strain was isolated from sediment from a river polluted by the AMD of an abandoned mine in Shanxi, China. Whole genome sequencing analyses revealed that the genome of *A. ferrooxidans* YQ-N3 includes one circular chromosome and five circular plasmids, among which one plasmid had not been annotated in public databases. *A. ferrooxidans* YQ-N3 is closely related to *A. ferrooxidans* ATCC23270 and *A. ferridurans* JCM18981, and its distribution of functional genes is similar to that of *A. ferrooxidans* ATCC23270 and *A. ferrooxidans* BY0502. This newly identified strain possesses multiple genes related to iron and sulfur metabolism. However, additional studies are required to characterize its energy metabolism pathways. The results of functional genome analysis and laboratory experiments jointly demonstrated that *A. ferrooxidans* YQ-N3 can accelerate the oxidation of $Fe^{2+}$, $S^0$, and $FeS_2$. Additionally, a 62.25% total sulfur removal rate was achieved in the biological coal desulfurization experiments conducted in this study. This study not only established a theoretical foundation for future research on the generation and treatment of AMD but also isolated a new bacterial strain that could be used for industrial desulfurization, biometallurgy, and the disposal of waste electronic products.

**Supplementary Materials:** The following supporting information can be downloaded at https://www.mdpi.com/article/10.3390/min13010095/s1, Table S1. General features and genomic comparison between *A. ferrooxidans* YQ-N3 and the other published genomes of *A. ferrooxidans*. Table S2. List of selected genes identified in the YQ-N3 strain via KEGG annotation, including genes for iron and sulfur metabolism.

**Author Contributions:** Conceptualization, Q.F.; investigation, W.L. and Z.L.; data analysis, W.L.; writing, W.L. All authors have read and agreed to the published version of the manuscript.

**Funding:** This research was supported by the National Natural Science Foundation of China (Grant No. 41977159; "Mechanism and kinetics of microbial acid inhibition in acid mine drainage of an abandoned coal mine").

**Data Availability Statement:** Not applicable.

**Acknowledgments:** We thank Beijing BMK Biological Co., Ltd. for conducting DNA sequencing.

**Conflicts of Interest:** The authors declare no conflict of interest.

## References


1. Zhan, Y.; Yang, M.R.; Zhang, S.; Zhao, D.; Duan, J.G.; Wang, W.D.; Yan, L. Iron and sulfur oxidation pathways of Acidithiobacillus ferrooxidans. *World J. Microbiol. Biotechnol.* **2019**, *35*, 12. [CrossRef] [PubMed]
2. Moinier, D.; Byrne, D.; Amouric, A.; Bonnefoy, V. The Global Redox Responding RegB/RegA Signal Transduction System Regulates the Genes Involved in Ferrous Iron and Inorganic Sulfur Compound Oxidation of the Acidophilic *Acidithiobacillus ferrooxidans*. *Front. Microbiol.* **2017**, *8*, 16. [CrossRef] [PubMed]
3. Zhang, S.; Yan, L.; Xing, W.J.; Chen, P.; Zhang, Y.; Wang, W.D. *Acidithiobacillus ferrooxidans* and its potential application. *Extremophiles* **2018**, *22*, 563–579. [CrossRef]
4. Iakovleva, E.; Mäkilä, E.; Salonen, J.; Sitarz, M.; Wang, S.B.; Sillanpää, M. Acid mine drainage (AMD) treatment: Neutralization and toxic elements removal with unmodified and modified limestone. *Ecol. Eng.* **2014**, *81*, 30–40. [CrossRef]
5. Valdes, J.; Pedroso, I.; Quatrini, R.; Dodson, R.J.; Tettelin, H.; Blake, R.; Eisen, J.A.; Holmes, D.S. *Acidithiobacillus ferrooxidans* metabolism: From genome sequence to industrial applications. *BMC Genom.* **2008**, *9*, 24. [CrossRef]
6. Lorenzo-Tallafigo, J.; Iglesias-González, N.; Mazuelos, A.; Romero, R.; Carranza, F. An alternative approach to recover lead, silver and gold from black gossan (polymetallic ore). Study of biological oxidation and lead recovery stages. *J. Clean. Prod.* **2019**, *207*, 510–521. [CrossRef]
7. Nie, H.Y.; Yang, C.; Zhu, N.W.; Wu, P.X.; Zhang, T.; Zhang, Y.Q.; Xing, Y.J. Isolation of *Acidithiobacillus ferrooxidans* strain Z1 and its mechanism of bioleaching copper from waste printed circuit boards. *J. Chem. Technol. Biotechnol.* **2015**, *90*, 714–721. [CrossRef]
8. Yang, M.R.; Zhan, Y.; Zhang, S.; Wang, W.D.; Yan, L. Biological materials formed by *Acidithiobacillus ferrooxidans* and their potential applications. *3 Biotech* **2020**, *10*, 9. [CrossRef]
9. Rout, P.G.; Mohanty, A.K.; Pradhan, N.; Biswal, S.K.; Behera, S.K. Study on the Reaction Mechanism of Oxidative Microbial Desulfurization of Organic Sulfur-Rich Coal. *Geomicrobiol. J.* **2022**, *39*, 210–218. [CrossRef]
10. Lavalle, L.; Chiacchiarini, P.; Pogliani, C.; Donati, E. Isolation and characterization of acidophilic bacteria from Patagonia, Argentina. *Process Biochem.* **2005**, *40*, 1095–1099. [CrossRef]
11. Kai, M.; Yano, T.; Fukumori, Y.; Yamanaka, T. Cytochrome oxidase of an acidophilic iron-oxidizing bacterium, *Thiobacillus ferrooxidans*, functions at pH 3.5. *Biochem. Biophys. Res. Commun.* **1989**, *160*, 839–843. [CrossRef] [PubMed]
12. Rhoads, A.; Au, K.F. PacBio Sequencing and Its Applications. *Genom. Proteom. Bioinform.* **2015**, *13*, 278–289. [CrossRef] [PubMed]
13. Delcher, A.L.; Bratke, K.A.; Powers, E.C.; Salzberg, S.L. Identifying bacterial genes and endosymbiont DNA with Glimmer. *Bioinformatics* **2007**, *23*, 673–679. [CrossRef]
14. Besemer, J.; Borodovsky, M. GeneMark: Web software for gene finding in prokaryotes, eukaryotes and viruses. *Nucleic Acids Res.* **2005**, *33*, W451–W454. [CrossRef] [PubMed]
15. Bertelli, C.; Laird, M.R.; Williams, K.P.; Lau, B.Y.; Hoad, G.; Winsor, G.L.; Brinkman, F.S.L.; Simon Fraser Univ Res Comp, G. IslandViewer 4: Expanded prediction of genomic islands for larger-scale datasets. *Nucleic Acids Res.* **2017**, *45*, W30–W35. [CrossRef] [PubMed]
16. Fouts, D.E. Phage_Finder: Automated identification and classification of prophage regions in complete bacterial genome sequences. *Nucleic Acids Res.* **2006**, *34*, 5839–5851. [CrossRef] [PubMed]
17. Bland, C.; Ramsey, T.L.; Sabree, F.; Lowe, M.; Brown, K.; Kyrpides, N.C.; Hugenholtz, P. CRISPR Recognition Tool (CRT): A tool for automatic detection of clustered regularly interspaced palindromic repeats. *BMC Bioinform.* **2007**, *8*, 8. [CrossRef]
18. Cury, J.; Jove, T.; Touchon, M.; Neron, B.; Rocha, E.P.C. Identification and analysis of integrons and cassette arrays in bacterial genomes. *Nucleic Acids Res.* **2016**, *44*, 4539–4550. [CrossRef]
19. Chen, J.J.; Liu, Y.L.; Diep, P.; Mahadevan, R. Genomic Analysis of a Newly Isolated *Acidithiobacillus ferridurans* JAGS Strain Reveals Its Adaptation to Acid Mine Drainage. *Minerals* **2021**, *11*, 14. [CrossRef]
20. Akcil, A.; Ciftci, H.; Deveci, H. Role and contribution of pure and mixed cultures of mesophiles in bioleaching of a pyritic chalcopyrite concentrate. *Miner. Eng.* **2007**, *20*, 310–318. [CrossRef]
21. Gonzalez-Toril, E.; Llobet-Brossa, E.; Casamayor, E.O.; Amann, R.; Amils, R. Microbial ecology of an extreme acidic environment, the Tinto river. *Appl. Environ. Microbiol.* **2003**, *69*, 6959. [CrossRef]
22. Umanskii, A.B.; Klyushnikov, A.M. Bioleaching of low grade uranium ore containing pyrite using *A. ferrooxidans* and *A. thiooxidans*. *J. Radioanal. Nucl. Chem.* **2013**, *295*, 151–156. [CrossRef]
23. Zhang, Y.; Zhang, S.; Zhao, D.; Ni, Y.Q.; Wang, W.D.; Yan, L. Complete Genome Sequence of *Acidithiobacillus ferrooxidans* YNTRS-40, a Strain of the Ferrous Iron- and Sulfur-Oxidizing Acidophile. *Microorganisms* **2020**, *8*, 10. [CrossRef]
24. Hinger, I.; Ansorge, R.; Mussmann, M.; Romano, S. Phylogenomic Analyses of Members of the Widespread Marine Heterotrophic Genus *Pseudovibrio* Suggest Distinct Evolutionary Trajectories and a Novel Genus, Polycladidibacter gen. nov. *Appl. Environ. Microbiol.* **2020**, *86*, 17. [CrossRef]
25. Hemme, C.L.; Green, S.J.; Rishishwar, L.; Prakash, O.; Pettenato, A.; Chakraborty, R.; Deutschbauer, A.M.; Van Nostrand, J.D.; Wu, L.Y.; He, Z.L.; et al. Lateral Gene Transfer in a Heavy Metal-Contaminated-Groundwater Microbial Community. *mBio* **2016**, *7*, 14. [CrossRef] [PubMed]
26. Acosta, M.; Beard, S.; Ponce, J.; Vera, M.; Mobarec, J.C.; Jerez, C.A. Identification of putative sulfurtransferase genes in the extremophilic *Acidithiobacillus ferrooxidans* ATCC 23270 genome: Structural and functional characterization of the proteins. *Omics* **2005**, *9*, 13–29. [CrossRef] [PubMed]

27. Mealman, T.D.; Blackburn, N.J.; McEvoy, M.M. Metal export by CusCFBA, the periplasmic Cu(I)/Ag(I) transport system of Escherichia coli. *Curr. Top. Membr.* **2012**, *69*, 163–196.
28. Chacon, K.N.; Perkins, J.; Mathe, Z.; Alwan, K.; Ho, E.N.; Ucisik, M.N.; Merz, K.M.; Blackburn, N.J. Trapping intermediates in metal transfer reactions of the CusCBAF export pump of *Escherichia coli*. *Commun. Biol.* **2018**, *1*, 11. [CrossRef]
29. Almarcegui, R.J.; Navarro, C.A.; Paradela, A.; Albar, J.P.; von Bernath, D.; Jerez, C.A. Response to copper of *Acidithiobacillus ferrooxidans* ATCC 23270 grown in elemental sulfur. *Res. Microbiol.* **2014**, *165*, 761–772. [CrossRef]
30. Wenbin, N.; Dejuan, Z.; Feifan, L.; Lei, Y.; Peng, C.; Xiaoxuan, Y.; Hongyu, L.; Nan, W.B.; Dejuan, L.Z.; Feifan, Y.; et al. Quorum-sensing system in *Acidithiobacillus ferrooxidans* involved in its resistance to $Cu^{2+}$. *Lett. Appl. Microbiol.* **2011**, *53*, 84–91. [CrossRef]
31. Popa, O.; Hazkani-Covo, E.; Landan, G.; Martin, W.; Dagan, T. Directed networks reveal genomic barriers and DNA repair bypasses to lateral gene transfer among prokaryotes. *Genome Res.* **2011**, *21*, 599–609. [CrossRef] [PubMed]
32. Polz, M.F.; Alm, E.J.; Hanage, W.P. Horizontal gene transfer and the evolution of bacterial and archaeal population structure. *Trends Genet.* **2013**, *29*, 170–175. [CrossRef]
33. Coutinho, T.J.D.; Franco, G.R.; Lobo, F.P. Homology-Independent Metrics for Comparative Genomics. *Comp. Struct. Biotechnol. J.* **2015**, *13*, 352–357. [CrossRef] [PubMed]
34. Dominguez-Mirazo, M.; Jin, R.; Weitz, J.S. Functional and comparative genomic analysis of integrated prophage-like sequences in "candidatus liberibacter asiaticus". *mSphere* **2019**, *4*, 409–419. [CrossRef] [PubMed]
35. Cady, K.C.; Bondy-Denomy, J.; Heussler, G.E.; Davidson, A.R.; O'Toole, G.A. The CRISPR/Cas Adaptive Immune System of Pseudomonas aeruginosa Mediates Resistance to Naturally Occurring and Engineered Phages. *J. Bacteriol.* **2012**, *194*, 5728–5738. [CrossRef] [PubMed]
36. Dopson, M.; Holmes, D.S. Metal resistance in acidophilic microorganisms and its significance for biotechnologies. *Appl. Microbiol. Biotechnol.* **2014**, *98*, 8133–8144. [CrossRef] [PubMed]
37. Nies, D.H. Efflux-mediated heavy metal resistance in prokaryotes. *Fems Microbiol. Rev.* **2003**, *27*, 313–339. [CrossRef]
38. Hemme, C.L.; Deng, Y.; Gentry, T.J.; Fields, M.W.; Wu, L.Y.; Barua, S.; Barry, K.; Tringe, S.G.; Watson, D.B.; He, Z.L.; et al. Metagenomic insights into evolution of a heavy metal-contaminated groundwater microbial community. *ISME J.* **2010**, *4*, 660–672. [CrossRef]
39. Hallberg, K.B.; Gonzalez-Toril, E.; Johnson, D.B. *Acidithiobacillus ferrivorans*, sp nov.; facultatively anaerobic, psychrotolerant iron-, and sulfur-oxidizing acidophiles isolated from metal mine-impacted environments. *Extremophiles* **2010**, *14*, 9–19. [CrossRef]
40. Bonnefoy, V.; Holmes, D.S. Genomic insights into microbial iron oxidation and iron uptake strategies in extremely acidic environments. *Environ. Microbiol.* **2012**, *14*, 1597–1611. [CrossRef]
41. Ponce, J.S.; Moinier, D.; Byrne, D.; Amouric, A.; Bonnefoy, V. Acidithiobacillus ferrooxidans oxidizes ferrous iron before sulfur likely through transcriptional regulation by the global redox responding RegBA signal transducing system. *Hydrometallurgy* **2012**, *127*, 187–194. [CrossRef]
42. Johnson, D.B.; Hallberg, K.B. Carbon, Iron and Sulfur Metabolism in Acidophilic Micro-Organisms. In *Advances in Microbial Physiology*; Poole, R.K., Ed.; Academic Press Ltd-Elsevier Science Ltd: London, UK, 2009; Volume 54, pp. 201–255.
43. Bird, L.J.; Bonnefoy, V.; Newman, D.K. Bioenergetic challenges of microbial iron metabolisms. *Trends Microbiol.* **2011**, *19*, 330–340. [CrossRef] [PubMed]
44. Yarzabal, A.; Appia-Ayme, C.; Ratouchniak, J.; Bonnefoy, V. Regulation of the expression of the *Acidithiobacillus ferrooxidans* rus operon encoding two cytochromes c, a cytochrome oxidase and rusticyanin. *Microbiology* **2004**, *150*, 2113–2123. [CrossRef] [PubMed]
45. Amouric, A.; Appia-Ayme, C.; Yarzabal, A.; Bonnefoy, V. Regulation of the iron and sulfur oxidation pathwayways in the acidophilic *A. Ferrooxidans*. *Adv. Mater. Res.* **2009**, *71–73*, 163–166. [CrossRef]
46. Kucera, J.; Bouchal, P.; Lochman, J.; Potesil, D.; Janiczek, O.; Zdrahal, Z.; Mandl, M. Ferrous iron oxidation by sulfur-oxidizing *Acidithiobacillus ferrooxidans* and analysis of the process at the levels of transcription and protein synthesis. *Antonie Van Leeuwenhoek* **2013**, *103*, 905–919. [CrossRef]
47. Wakai, S.; Tsujita, M.; Kikumoto, M.; Manchur, M.A.; Kanao, T.; Kamimura, K. Purification and characterization of sulfide: Quinone oxidoreductase from an acidophilic iron-oxidizing bacterium, acidithiobacillus ferrooxidans. *Biosci. Biotechnol. Biochem.* **2007**, *71*, 2735–2742. [CrossRef]
48. Liu, Y.D.; Ji, J.J.; Yu, R.L.; Qiu, G.Z. Expression, Purification and Molecular Modeling of Another HdrC from *Acidithiobacillus ferrooxidans* Which Binds Only One 4Fe-4S Cluster. *Curr. Microbiol.* **2012**, *65*, 416–423. [CrossRef]
49. Offeddu, F.G.; Cama, J.; Soler, J.M.; Dávila, G.; McDowell, A.; Craciunescu, T. Processes affecting the efficiency of limestone in passive treatments for AMD: Column experiments. *J. Environ. Chem. Eng.* **2015**, *3*, 304–316. [CrossRef]
50. Nazari, B.; Jorjani, E.; Hani, H.; Manfi, Z.; Riahi, A. Formation of jarosite and its effect on important ions for *A. ferrooxidan*s bacteria. *Trans. Nonferrous Met. Soc. China* **2014**, *24*, 1152–1160. [CrossRef]
51. Li, W.B.; Feng, Q.Y.; Liang, H.Q.; Chen, D.; Li, X.D. Passive treatment test of acid mine drainage from an abandoned coal mine in Kaili Guizhou, China. *Water Sci. Technol.* **2021**, *84*, 1981–1996.
52. Konishi, Y.; Asai, S.; Yoshida, N. Growth Kinetics of *Thiobacillus thiooxidans* on the Surface of Elemental Sulfur. *Appl. Environ. Microbiol.* **1995**, *61*, 3617–3622. [CrossRef]

53. Knickerbocker, C.; Nordstrom, D.K.; Southam, G. The role of "blebbing" in overcoming the hydrophobic barrier during biooxidation of elemental sulfur by *Thiobacillus thiooxidans*. *Chem. Geol.* **2000**, *169*, 425–433. [CrossRef]
54. Kuang, J.L.; Huang, L.N.; Chen, L.X.; Hua, Z.S.; Li, S.J.; Hu, M.; Li, J.T.; Shu, W.S. Contemporary environmental variation determines microbial diversity patterns in acid mine drainage. *ISME J.* **2013**, *7*, 1038–1050. [CrossRef] [PubMed]
55. Cardona, I.C.; Marquez, M.A. Biodesulfurization of two Colombian coals with native microorganisms. *Fuel Process. Technol.* **2009**, *90*, 1099–1106. [CrossRef]
56. Yang, X.; Wang, S.; Liu, Y.; Zhang, Y. Identification and characterization of *Acidithiobacillus ferrooxidans* YY2 and its application in the biodesulfurization of coal. *Can. J. Microbiol.* **2015**, *61*, 65–71. [CrossRef]
57. Yang, X.P.; Wang, S.M.; Liu, Y.J.; Liang, Y. A Comparative Study of the Biodesulfurization Efficiency of *Acidithiobacillus ferrooxidans* LY01 Cells Domesticated with Ferrous Iron and Pyrite. *Geomicrobiol. J.* **2016**, *33*, 488–493. [CrossRef]
58. Newman, D.K. Feasting on Minerals. *Science* **2010**, *327*, 793–794. [CrossRef]
59. Liu, F.W.; Lei, Y.S.; Shi, J.; Zhou, L.X.; Wu, Z.H.; Dong, Y.; Bi, W.L. Effect of microbial nutrients supply on coal bio-desulfurization. *J. Hazard. Mater.* **2020**, *384*, 10. [CrossRef]
60. Arslan, V. The application of combined lignite cleaning processes, bacterial leaching and flotation, for reducing higher ash and sulfur contents. *Int. J. Coal Prep. Util.* **2022**, *42*, 2114–2126. [CrossRef]
61. Silva, R.A.; Park, J.; Ilyas, S.; Borja, D.; Zhao, H.B.; Urik, M.; Rastegar, S.O.; Kim, H. Biodegradation mechanism of arsenopyrite mine tailing with *Acidithiobacillus ferrooxidans* and influence of ferric supplements. *Int. Biodeterior. Biodegrad.* **2020**, *153*, 6. [CrossRef]
62. Schippers, A. Sand, Bacterial leaching of metal sulfides proceeds by two indirect mechanisms via thiosulfate or via polysulfides and sulfur. *Appl. Environ. Microbiol.* **1999**, *65*, 319–321. [CrossRef] [PubMed]
63. Chen, Z.H.; Huang, X.Y.; He, H.; Tang, J.L.; Tao, X.X.; Huang, H.Z.; Haider, R.; Ali, M.I.; Jamal, A.; Huang, Z.X. Bioleaching Coal Gangue with a Mixed Culture of *Acidithiobacillus ferrooxidans* and *Acidithiobacillus thiooxidans*. *Minerals* **2021**, *11*, 11. [CrossRef]